

pubs.acs.org/JPCB Article

Breakdown of the Stokes-Einstein Equation for Solutions of Water in Oil Reverse Micelles

Markus M. Hoffmann,* Matthew D. Too, Michael Vogel, Torsten Gutmann, and Gerd Buntkowsky*



Cite This: J. Phys. Chem. B 2020, 124, 9115–9125



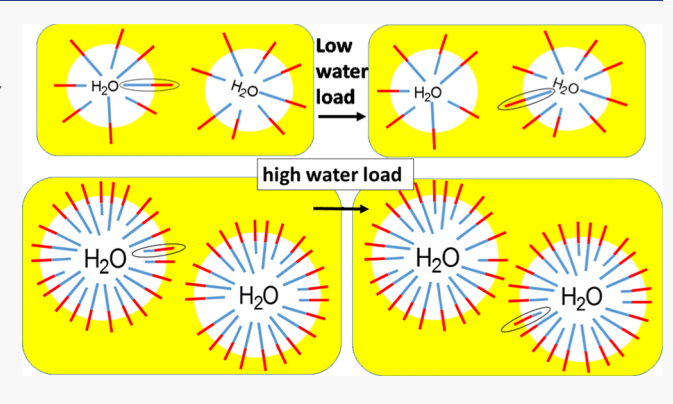
ACCESS I

Metrics & More

Article Recommendations

SI Supporting Information

ABSTRACT: An experimental study is presented for the reverse micellar system of 15% by mass polydisperse hexaethylene glycol monodecylether ($C_{10}E_6$) in cyclohexane with varying amounts of added water up to 4% by mass. Measurements of viscosity and self-diffusion coefficients were taken as a function of temperature between 10 and 45 °C at varying sample water loads but fixed $C_{10}E_6$ /cyclohexane composition. The results were used to inspect the validity of the Stokes–Einstein equation for this system. Unreasonably small reverse average micelle radii and aggregation numbers were obtained with the Stokes–Einstein equation, but reasonable values for these quantities were obtained using the ratio of surfactant-to-cyclohexane self-diffusion coefficients. While bulk viscosity increased with increasing water load, a concurrent



expected decrease of self-diffusion coefficient was only observed for the surfactant and water but not for cyclohexane, which showed independence of water load. Moreover, a spread of self-diffusion coefficients was observed for the protons associated with the ethylene oxide repeat unit in samples with polydisperse $C_{10}E_6$ but not in a sample with monodisperse $C_{10}E_6$. These findings were interpreted by the presence of reverse micelle to reverse micelle hopping motions that with higher water load become increasingly selective toward $C_{10}E_6$ molecules with short ethylene oxide repeat units, while those with long ethylene oxide repeat units remain trapped within the reverse micelle because of the increased hydrogen bonding interactions with the water inside the growing core of the reverse micelle. Despite the observed breakdown of the Stokes–Einstein equation, the temperature dependence of the viscosities and self-diffusion coefficients was found to follow Arrhenius behavior over the investigated range of temperatures.

■ INTRODUCTION

Surface-activating agents (surfactants) are amphiphilic molecules that form the basis of surface and colloid sciences. Surfactants form aggregates in solution, micelles in polar solvents such as water, and reverse micelles in nonpolar solvents. In this way, surfactants can solubilize into their aggregate core solutes that otherwise would be completely immiscible in the solvent, that is, micelles are able to dissolve nonpolar solutes in water, while polar solutes can be solubilized into reverse micelles dissolved in a nonpolar solvent.²

Reverse micelles play a prominent role in a variety of technologies such as biotechnology for the extraction of biomolecules, the delivery of drugs and as models for biological systems, 2-6 and in nanotechnology, 2-4 where nanostructures with controlled morphology and narrow size distributions can be achieved. Knowledge about the characteristics of the reverse micelle structure such as the average diameter and aggregation number (the number of surfactant molecules in a reverse micelle) is therefore desirable. One experimental approach that has been used to obtain such structural information of reverse micelles in nonpolar solvents is to measure the self-diffusion coefficient, *D*, using fluorescence

correlation spectroscopy, or, as is the focus in this report, NMR spectroscopy. In conjunction with the solution viscosity, η , taken either from literature of the pure solvent or more accurately measured directly for the micellar solutions, access to the desired average radius of the reverse micelle can principally be obtained through the well-known Stokes—Einstein equation

$$r = \frac{k_{\rm B}T}{c\pi\eta D} \tag{1}$$

where $k_{\rm B}$ is the Boltzmann constant, T the temperature in Kelvin, and c is a constant. Some reported investigations were modifying the Stokes–Einstein equation to take into account the possible nonspherical shape of the reverse micelle. However, we caution that details on micelle shape may not be

Received: July 4, 2020
Revised: September 11, 2020
Published: September 14, 2020





accessible because of the long time scale of NMR measurements. Specifically, the NMR self-diffusion coefficients represent an ensemble and time average of the self-diffusion of all present species in dynamic equilibrium. For reverse micellar systems, it has been shown that the formation of reverse micelles S_n from surfactant S may proceed in a stepwise equilibria, that is, $S+S\rightleftharpoons S_2$, $S+S_2\rightleftharpoons S_3$, $S+S_3\rightleftharpoons S_4$, and so forth, where each equilibrium has its respective corresponding equilibrium constant. Even the concentration of single surfactant molecules may not be negligible. For example, there was evidence from small-angle neutron scattering measurements that a nonionic surfactant of the type C_mE_n (Scheme 1) showed a gradual transition from individually dissolved surfactant molecules to the formation of reverse micelles. 16

Scheme 1. Structure of $C_m E_n$ Poly(ethylene oxide) Alcohol, where m Represents the Number of Carbon Atoms in the Alkyl Chain and n is the Number of Ethylene Oxide Repeat Units

In this regard, a recent study of reverse micelles of C₁₀E₆ in cyclohexane used combined measurements of NMR selfdiffusion, viscosity, and melting point depression to characterize the speciation and average reverse micelle size as a function of C₁₀E₆ concentration.¹⁷ Unreasonably small radii and thus aggregation numbers were obtained when using the Stokes-Einstein equation with worsening trend as the surfactant concentration was increased. However, reasonable radii and aggregation numbers were obtained when using a simple calculation based on the ratio of C₁₀E₆ and cyclohexane selfdiffusion coefficients. This interesting finding sparked the investigations presented in this report. Specifically, the main goal of this study at the outset was to determine if similar trends would also be observed when the water load in this reverse micellar system would be increased. The rationale behind this goal is that water, which is an omnipresent impurity in the typically hygroscopic surfactants, 18 is known to act as a nucleation site of micelle formation,² and addition of water leads to a swelling of the reverse micelles. ^{7,8,11,14,19,20} In fact, the water confined within the polar reversed micellar core is often referred to as a water pool, in which even chemical synthesis can be carried out. 15,20,21 Hence, we anticipated that the Stokes-Einstein equation would also progressively lead to unreasonably small aggregation numbers with increasing water load. As we will show, the results in this report confirm this anticipated failure of the Stokes-Einstein equation, while the ratio of surfactant and solvent self-diffusion coefficients lead to aggregation numbers more in line with literature values. These findings should be of broad interest in the context of limits of the Stokes-Einstein equation because a breakdown of the Stokes-Einstein equation is by no means a new phenomenon. It has been observed in many systems, foremost in supercooled liquids, where diffusivity and viscosity show different temperature dependencies when the glass-transition temperature T_{g} is approached.^{22,23} Recent studies hereto include metal alloys, ^{24–31} some of which are of technological interest as phase-change materials, ^{32–34} acebutolol hydrochloride, ³⁵ polymer melts, 36-38 some ionic liquids, 39-41 supercooled

water, ^{42–44} and solutions of lithium perchlorate in polyethylene glycols. ⁴⁵ Pronounced deviations from the Stokes—Einstein equation have also been observed in binary systems for which one would ordinarily expect the Stokes—Einstein equation to hold. Recent examples include aqueous lithium chloride solutions, ^{46,47} glycerol, ⁴⁸ dimethylsulfoxide, ^{49,50} ethanol, ⁴⁹ some eletrolytes, ⁵¹ tetraethyleneglycol in levitated viscous aerosols, ⁵² and small molecules in supercritical water. ⁵³ Turton and Wynne even questioned if deviations from the closely related Stokes—Einstein—Debye equation for molecular orientational diffusion are the rule rather than the exception based on their Kerr-effect spectroscopy study on guanidine hydrochloride in water and mixtures of carbon disulfide with hexadecane. ⁵⁴ Thus, this report will include perspectives from these studies in the discussions of the presented findings.

The organization of the remainder of this report is as follows: details on sample preparation and density, viscosity, and self-diffusion measurements are provided in the Methods section. The results, including comments on measurement accuracy and precision, are presented separately from the Discussion section in the Results section. Thus, the Discussion section focuses on the interpretation of the results within the context of findings reported in the literature on other systems that do not follow the Stokes–Einstein equation. The paper finishes with concluding remarks in the Conclusions section.

METHODS

Chemicals and Solution Preparation. Solutions were prepared such that the molality of C₁₀E₆ in cyclohexane was constant for all samples at 0.406 mol C₁₀E₆ per kg⁻¹ cyclohexane, which corresponds to 15% by mass C₁₀E₆ in cyclohexane. The cyclohexane (reagent grade ACS, 99% mass purity) was purchased from Pharmco-Aaper and the polydisperse nonionic surfactant C₁₀E₆ was generously donated by Rochester Midland Corporation, who purchased the chemical in large quantities from Air Products. The exact composition of the polydisperse C₁₀E₆ has previously been analyzed and can be found in the Supporting Information of Hoffmann et al.⁵⁵ One sample for self-diffusion measurements only was also prepared with monodisperse $C_{10}E_6$ obtained from Santa Cruz Biotechnology with a purity of 99% or better. Distilled water was purified by a Thermo Scientific Barnstead UV Purification System to a specific resistance of 18.3 M Ω ·cm. The water load of the polydisperse C₁₀E₆ was determined to be $(3.4 \pm 0.2) \times 10^{-3}$ mass fraction by a METTLER TOLEDO Karl Fischer frit-less titrator in three replicates. An electronic balance with a precision of 1×10^{-4} g was used to weigh out all components. Solutions were prepared in sample vials by mixing C₁₀E₆ and water with vigorous shaking to achieve a homogeneous, clear fluid mixture. Cyclohexane was added thereafter. Further vigorous shaking was carried out to uniformly mix components and allow for the equilibration of C₁₀E₆ reverse micelle formation. The specific solution composition details can be found in Table S1, where the water content is reported as percent by mass relative to mass of the total solution and accounts for the water impurity load present in C₁₀E₆. Density, viscosity, and self-diffusion measurements were generally all obtained from the exact same samples.

Viscosity and Density Measurements. An Anton Paar AMVn rolling ball microviscometer and Anton Paar vibrating U-tube densitometer with Peltier temperature controls of precision of 0.02 K were run in parallel to determine the

viscosities and densities, respectively, of prepared solutions. A 1.6 mm capillary, calibrated against boiled ultrapure water (Anton Paar lot 1012), was used for viscosity measurements. Viscosity and density measurements were acquired within 24 h of solution preparation at temperatures of 10-45 °C in increments of 5 °C at angles of 30, 40, and 50° with six repetitions per angle. Samples were confined during measurements, that is, not exposed to the laboratory atmosphere. Each experiment was started and completed with a temperature of 20 °C, and the results were comparable within measurement uncertainty except for the 4% water sample as further noted in the Results section. For all solutions, viscosities and their standard deviations are reported based on at least 12 repeated measurements. Density measurements were all repeatable to 0.0001 g/cm³, which thus is taken as the standard deviation for each of the reported density values.

NMR Self-Diffusion Measurements. Diffusion-ordered spectroscopy (DOSY) measurements were carried out on an AVANCE 300 NMR instrument from Bruker BioSpin with a variable temperature broadband probe with temperature precision of 0.1 °C. The instrument was calibrated for temperature using the known temperature dependencies of ethylene glycol chemical shifts.⁵⁶ Prepared solutions were held in valve-containing NMR tubes and analyzed at temperatures of 10-45 °C in increments of 5 °C using cold boil-off gas from liquid nitrogen for cooling or compressed air for heating. Flame-sealed Pyrex capillaries containing D2O were inserted into the NMR tubes for use as the lock signal. The temperature was equilibrated for at least 15 min before data acquisition. For all samples, the NMR tubes were not spun, and shimming and receiver gain settings were optimized accordingly. A pulse program using a double stimulated echo with bipolar gradients and three spoil gradients was used. 57,58 Acquisitions were conducted with delays of 5 s for relaxation, 5 ms for eddy current recovery, and 0.2 ms for gradient recovery, respectively. To determine the self-diffusion coefficients for each solution component, the stimulated spin-echo intensity, I(g), was plotted as a function of magnetic field gradient strength, g, according to the equation⁵⁹

$$I(g) = I_0 e^{-D\gamma^2 g^2 \delta^2 ((4\Delta - \delta)/\pi^2)}$$
 (2)

where I_0 is the reference spin-echo intensity in the absence of gradient, γ is the ¹H gyromagnetic ratio, and Δ is the diffusion time of 0.1 s. Because self-diffusion coefficients were found to differ substantially between cyclohexane and $C_{10}E_6$ (and water), it was necessary to conduct self-diffusion measurements separately for cyclohexane and C₁₀E₆ with gradient pulse duration, δ , optimized for cyclohexane and $C_{10}E_6$, respectively. A total of 16 scans corresponding to 16 sine-shaped gradient pulses from 0.35 to 3.5 g mm⁻¹ gradient strength in linear or squared increments were used. Four dummy scans were used prior to the 16 scans to acquire steady-state conditions. The self-diffusion coefficients for each constituent were obtained by fitting eq 2 to the I(g) data, where I(g) values were found by integrating respective spectral peaks. The self-diffusion coefficients for C₁₀E₆ and their standard deviations were determined as the average from multiple C₁₀E₆ spectral features. For the self-diffusion coefficients of cyclohexane, a relative standard deviation value of 2% was found from repeating measurements on a few select samples. Because water was found to diffuse much slower than cyclohexane, the

relative standard deviation of the water self-diffusion coefficients were much higher, but no more, than 10%.

RESULTS

Viscosities. Measurement results of viscosity, η , for the 15% by mass polydisperse $C_{10}E_6$ in cyclohexane system with various amounts of added water are summarized in Table S2, and their respective uncertainties are listed in Table S3. Viscosities increase gradually with water load but rise sharply from 3 to 4% added water. In this respect, indication of a possible slight temperature hysteresis was noted in the data series for 4 mass% of water. Independent solubility tests showed that liquid—liquid phase separation occurs upon addition of 6–7% by mass of water. Therefore, sample preparation and measurements for the 4% water sample were repeated to confirm data reproducibility. Although variations are larger than the standard deviations listed in Table S3, the results are in reasonable agreement.

The logarithmic form of the Arrhenius equation is shown in eq 3

$$\ln(X(T)) = \ln A \pm \frac{E_{a}}{RT}$$
(3)

where X(T) represents the temperature-dependent quantity of interest, A is the pre-exponential factor, $E_{\rm a}$ is the activation energy, and R is the gas constant. When plotting $\ln(X(T))$ as a function of 1/T, the sign of the slope is positive for viscosity but negative for self-diffusion coefficients, which is reflected by the \pm sign in the right-hand side of eq 3. The temperature dependence of the viscosity shows Arrhenius behavior for all studied samples over the investigated temperature range as evidenced in Figure 1 showing graphs of $\ln(\eta)$ versus inverse

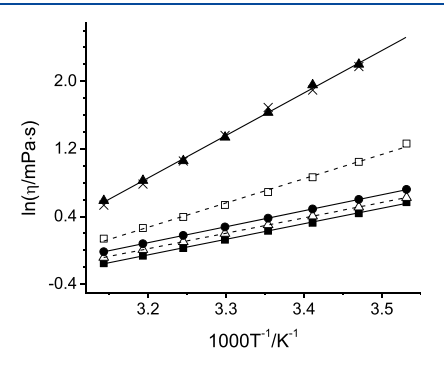


Figure 1. Arrhenius plot of $\ln(\eta)$ vs inverse temperature for 15% by mass polydisperse $C_{10}E_6$ in cyclohexane with least-squares fits for 0 (\blacksquare), 1 (\triangle), 2 (\blacksquare), 3 (\square), and 4 (\blacktriangle) % by mass added water. The 4% by mass measurement series was repeated (\times) where the measurement at 0.00357 K^{-1} needed to be omitted because of instrument limitations.

temperature. As can be seen in the fit parameters summarized in Table 1, the slopes and thus the activation energies become substantially larger at higher mass percent of added water (\sim 50% increase from 2 to 3% added water and \sim 75% increase from 3 to 4% added water).

Self-Diffusion Coefficients. Figure S1 shows an exemplary proton spectrum for 15% polydisperse $C_{10}E_6$ in cyclohexane with 3 mass percent added water at 15 $^{\circ}C$ and provides a spectral assignment. Because of the fast chemical exchange, only one peak is observed for water and hydroxyl protons. The cyclohexane resonance overlaps with the

Table 1. Arrhenius Analysis of Viscosity for 15% by Mass Polydisperse $C_{10}E_6$ in Cyclohexane System with Varying Added Mass % of Water

% H ₂ O	0	1	2	3	4
Intercept	-5.9460	-5.8100	-5.9631	-8.9208	-15.239
slope/K	1841.2	1821.6	1891.5	2872.9	5029.4
R^2	0.9993	1.0000	1.0000	0.9966	0.9987
$E_{\rm a}/{\rm kJ\cdot mol^{-1}}$	15.3 ± 0.2	15.15 ± 0.01	15.73 ± 0.03	23.9 ± 0.6	41.8 ± 0.7

methylene protons of the surfactant alkyl chain but is so dominant that interference with the self-diffusion measurement of cyclohexane is limited.

When conducting NMR self-diffusion measurements, a spectrum is obtained under varying field gradient strengths. According to eq 2, the intensity of a spectral feature as a function of applied field gradient strength should be a Gaussian function. However, for the spectral feature near 3.7 ppm representing the ethylene oxide repeat unit in $C_{10}E_6$, increasing deviations from a Gaussian function are observed with increasing water load, as exemplary illustrated in the Supporting Information in Figures S2-S6. The 2D representations of these NMR self-diffusion data sets, referred to as 2D-DOSY plots, are showing indeed a spread of the polyethylene oxide spectral feature to slower self-diffusion coefficients than for the other C₁₀E₆ spectral features. This spread is not observed for any of the other spectral features for water, cyclohexane, and the other spectral features of C₁₀E₆ such as its terminal methyl group, as exemplary illustrated in Figure 2.

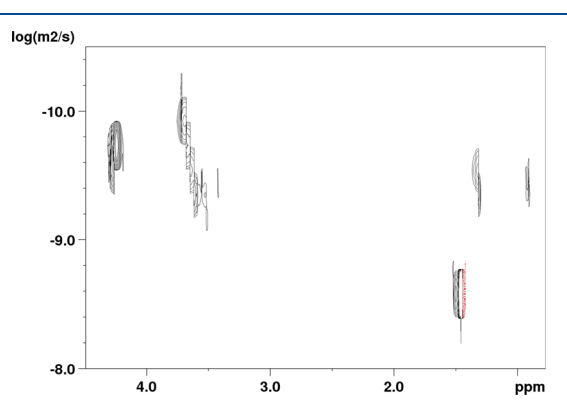


Figure 2. Two-dimensional DOSY spectrum showing the base-10 logarithm of the self-diffusion coefficient vs the proton chemical shift for polydisperse 15% $C_{10}E_6$ in cyclohexane with four mass percent water at 45 °C. The cross peaks at 1.5 and 4.2 ppm are representative for cyclohexane and water, respectively. All other cross peaks are from polydisperse $C_{10}E_6$, where only the signals at 3.5–3.7 ppm for the ethylene oxide repeat unit show a spread of self-diffusion coefficients. For a detailed spectral assignment, see Figure S1 in the Supporting Information.

This observation is remarkable in so far that a molecule should self-diffuse as a unit. Consequently, all spectral features representing the same molecule should show the same self-diffusion coefficients. However, when repeating the self-diffusion measurement with a similar sample except using monodisperse rather than polydisperse $C_{10}E_6$, the spread of the $C_{10}E_6$ polyethylene oxide signal in the 2D-DOSY spectrum is absent, as exemplary shown in Figure S7 in the Supporting Information.

Given these described peculiarities for the polydisperse $C_{10}E_6$ self-diffusion data, the accuracy of the reported average self-diffusion coefficients of polydisperse $C_{10}E_6$ may be limited,

and the obtained standard deviations obtained from averaging the self-diffusion coefficients from the various polydisperse $C_{10}E_6$ spectral features are also quite large, as can be seen in Table S5. However, when repeating measurements multiple times for selected conditions (35 °C entries in Table S4), the obtained self-diffusion coefficients are reproducible, and scatter is significantly less than the standard deviations reported in Table S5. The self-diffusion coefficients obtained from the sample with monodisperse $C_{10}E_6$ are 15–35% higher than the corresponding self-diffusion coefficients from the sample with polydisperse $C_{10}E_6$.

The temperature dependence of the $C_{10}E_6$ self-diffusion coefficients for each of the five samples with polydisperse $C_{10}E_6$ appears to show Arrhenius behavior over the investigated temperature range as illustrated in Figure 3. The

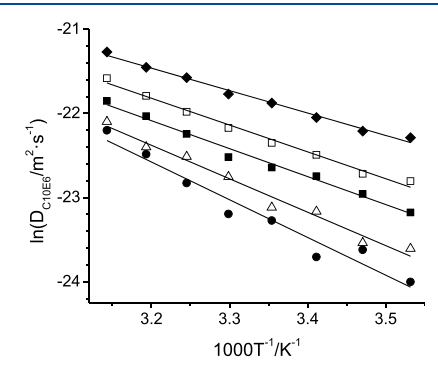


Figure 3. Arrhenius plot of $\ln(D_{C_{10}E_6})$ vs inverse temperature with least-squares fits for solutions of 0 (\spadesuit), 1 (\square), 2 (\blacksquare), 3 (\triangle), and 4 (\bullet) mass percent water.

results of the linear least-squares fit parameters are summarized in Table 2. The magnitude of the slopes in the graphs of Figure 3 and thus the activation energies gradually increase with increasing water load in the sample.

The self-diffusion coefficients of cyclohexane and water/OH for systems containing polydisperse C₁₀E₆ are reported in Tables S6 and S7, respectively. The cyclohexane self-diffusion coefficients are as expected significantly larger than the corresponding self-diffusion coefficents for C₁₀E₆. The selfdiffusion coefficients for water/OH are overall slightly lower than the corresponding values in Table S4 for C₁₀E₆. These trends can also be seen by the vertical positions of the spectral features in the exemplary 2D-DOSY plot in Figure 2. One remarkable observation for cyclohexane self-diffusion coefficients is that they depend only on temperature and are essentially independent of water load. This can be seen in the Arrhenius plots for the temperature-dependent cyclohexane self-diffusion coefficients shown in Figure 4, where the data points essentially overlap. In contrast, the water self-diffusion coefficients are dependent on water load as can be in the two exemplary Arrhenius plots shown in Figure 4. The results of the least-squares linear regressions for the Arrhenius analysis of

Table 2. Arrhenius Analysis of Self-Diffusion Coefficients for 15% by Mass Polydisperse $C_{10}E_6$ in Cyclohexane System with Varying Added Mass% of Water

% H ₂ O	0	1	2	3	4
		Cyclol	nexane		
intercept	-14.88	-14.70	-15.06	-14.70	-14.52
slope/K	-1691	-1736	-1627	-1744	-1798
R^2	0.994	0.995	0.995	0.996	0.997
$E_a/kJ \cdot mol^{-1}$	14.1 ± 0.5	14.4 ± 0.4	13.5 ± 0.4	14.5 ± 0.4	15.0 ± 0.3
		C_{10}	$_{0}E_{6}$		
intercept	-12.90	-11.65	-11.44	-9.41	-8.40
slope/K	-2674	-3180	-3329	-4050	-4436
R^2	0.992	0.990	0.987	0.973	0.958
$E_a/kJ \cdot mol^{-1}$	22.2 ± 0.7	26.4 ± 0.9	27.7 ± 1.1	33.7 ± 1.9	36.9 ± 2.6
		Wa	ter		
intercept		-13.79	-10.27	-10.05	-13.06
slope/K		-2544	-3795	-3979	-3055
R^2		0.960	0.988	0.997	0.988
$E_a/kJ \cdot mol^{-1}$		21.2 ± 1.8	31.5 ± 1.4	33.1 ± 0.7	25.4 ± 1.1

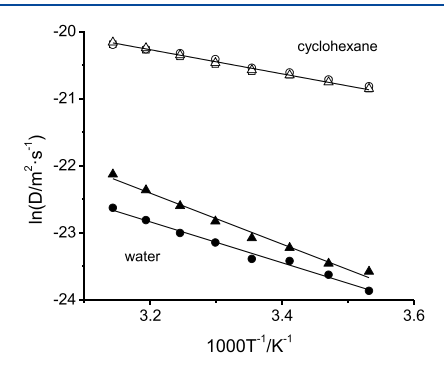


Figure 4. Arrhenius plots of $\ln(D)$ vs inverse temperature for the cyclohexane component in 15% polydisperse $C_{10}E_6$ in cyclohexane solutions with added 0 (\square), 2 (\triangle), and 4 (\bigcirc) mass percent water and for the water component at 2 (\blacktriangle) and 4 (\bigcirc) mass percent water. The lines are from linear regressions, where in the case of the cyclohexane component only the fit line for the data from the 4 mass percent water sample is shown.

the cyclohexane and water self-diffusion coefficients are summarized in Table 2.

Micelle Radii and Aggregation Numbers. As explained in the introduction, a key motivation for this study on $C_{10}E_6$ reverse micelles in cyclohexane as a function of water load was to inspect the validity of (a) the Stokes–Einstein equation and (b) the ratio of cyclohexane and surfactant self-diffusion coefficients, $D_{C_6H_{12}}/D_{C_{10}E_6}$, to obtain average reverse micelle radii. Thus, the same evaluations to obtain radii in these two ways were carried out here as described previously 17 using eqs 1, 4, and 5, where here too a value of 2.90 Å was taken for $r_{C_6H_{12}}$. The expression in eq 4 has been derived by Chen and Chen 60 from the microfriction theory by Gierer and Wirtz. 61

$$c = \frac{6}{1 + 0.695 \left(\frac{r_{C_6 H_{12}}}{r}\right)^{2.234}} \tag{4}$$

$$r = r_{C_6 H_{12}} \frac{D_{C_6 H_{12}}}{D_{C_{10} E_6}} \tag{5}$$

The radii obtained by eqs 1 and 4 using the surfactant self-diffusion coefficients are listed in Table S8, and the radii obtained by eq 5 are listed in Table S9. Corresponding

uncertainties estimated from error propagation calculations are shown, respectively, in Tables S10 and S11 in the Supporting Information. Exemplary radii are shown as a function of water load in Figure 5. In Figure 5, it can be seen that the radii

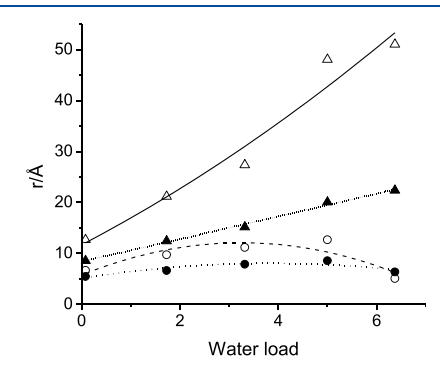


Figure 5. Average polydisperse $C_{10}E_6$ speciation radii as a function of water load at 15 °C (open symbols) and at 45 °C (filled symbols). The circles represent the radii using the Stokes–Einstein equation (eq 1). The triangles represent the radii obtained by using the ratio of $C_{10}E_6$ and cyclohexane self-diffusion coefficients (eq 5). The lines are guides to the eye.

obtained from the Stokes–Einstein equation are much smaller than the radii obtained from the ratio of the self-diffusion coefficients. The radii from the Stokes–Einstein equation also undergo a maximum with increasing water load present. This is not observed for the radii obtained from the ratio of self-diffusion coefficients. We note that the uncertainties for the radii obtained from eq 5 (Table S11) become rather large at the lowest temperatures for the samples of 3 and 4 mass% water. For these samples and temperature conditions, the $C_{10}E_6$ self-diffusion coefficients are smallest and thus, with same absolute measurement uncertainty, the relative standard deviations increase. However, the trend in Figure 5 of continual increase in these radii persists for all temperatures.

The aggregation numbers of $C_{10}E_6$ reverse micelles were estimated from the radii with eq 6 as done in other works 62,63

$$N = \frac{4\pi r^3}{3\left(\frac{[H_2O]}{[C_{10}E_6]}V_{H_2O} + V_{C_{10}E_6}\right)}$$
(6)

where $V_{\rm H_2O}$ and $V_{\rm C_{10}E_6}$ are the molecular volumes of water and $\rm C_{10}E_6$. These volumes were taken as the van der Waals volumes of 18.6 and 447.43 ų, respectively, obtained by the method by Bondi. The needed solution densities to evaluate the concentrations of water and $\rm C_{10}E_6$ for eq 6 were measured and are listed in Table S12. The resulting aggregation numbers using the Stokes–Einstein radii are listed in Table S13, and the aggregation numbers from the self-diffusion coefficient ratio radii are listed in Table S14 of the Supporting Information. The latter are plotted in Figure 6 as a

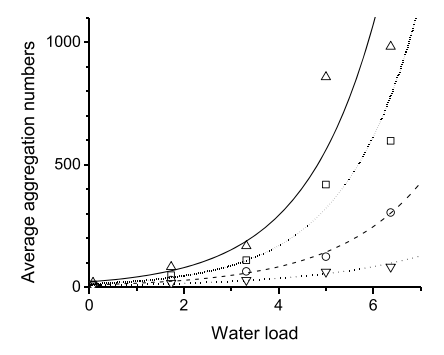


Figure 6. Average $C_{10}E_6$ aggregation numbers based on radii obtained from the ratio of self-diffusion coefficients $D_{C_6H_{12}}/D_{C_{10}E_6}$ at 15 °C (\triangle), 25 °C (\square), 35 °C (\bigcirc), and 45 °C (∇) with respect to water load ($W = [\text{water}]/[C_{10}E_6]$). The lines are guides to the eyes.

function of water load ($W = [H_2O]/[C_{10}E_6]$). The aggregation number increases in an exponential fashion with water load. The aggregation numbers for 0% added water reproduce the values reported in our previous study.¹⁷

Vasilescu et al. reported for the reverse micellar system of 15% C₁₂E₄ in cyclohexane at 8 °C an average aggregation number of 45 when 1% by mass water was added and 67 when 2% by mass water was added. 14 The concentration of 15% C₁₀E₆ in cyclohexane was chosen for this study to facilitate comparison with these results. The average aggregation numbers from the self-diffusion coefficient ratios for a 15% polydisperse C₁₀E₆ in cyclohexane solution at 10 °C are 83 and 240 with 1 and 2% by mass added water, respectively. While these values are larger than the ones reported by Vasilescu for C₁₂E₄, they are reasonable. In contrast, the radii from the Stokes-Einstein equation are much smaller than the radii from the ratio of self-diffusion coefficients and undergo a maximum near 3% added water, and the corresponding aggregation number reaches values only on the order of 10 and become unreasonably small for the sample of 4% added water. Aggregation numbers on the order of several hundreds were also reported for reverse micelles in cyclohexane with the related surfactant Igepal.³ Likewise, average reverse micelle radii obtained from dynamic light scattering (DLS) for the related surfactant Brij L-4 in hexane were reported to be between 20 and 50 Å for water loads between 1 and 6, in good agreement with the radii from the self-diffusion coefficients in Figure 5.66 The group of Aramaki extensively studied with DLS reverse micelles of glycerol monolaurate-based nonionic surfactants in various nonpolar solvents ^{19,67} including cyclohexane. ^{68–70} From these reports, it is evident that the nature of the nonpolar solvent significantly affects the micelle size in these systems and that the shape of the reverse micelle becomes increasingly nonspherical with increased size. For cyclohexane, the maximum largest dimension (diameter) of the reverse micelle with these nonionic surfactants at 5% by mass ranges between 30 and 100 Å depending on the specific surfactant and conditions of temperature, again with similar values as the radii from the self-diffusion coefficients in Figure 5.

In summary, the main remarkable results and findings that require deeper discussion in the next section are as follows. The cyclohexane self-diffusion coefficients are not dependent on the amount of added water, while the self-diffusion coefficients of the surfactant and water decrease with increased amount of added water. The polyethylene oxide resonance signals for the polydisperse $C_{10}E_6$ show nonuniformity in the 2D-DOSY plot, while such a spread is absent in the 2D-DOSY plot for a sample of monodisperse C₁₀E₆. The self-diffusion coefficients of all three components—cyclohexane, C₁₀E₆, and water-show Arrhenius behavior for the investigated temperature range. Average aggregate radii and aggregation numbers obtained from the Stokes-Einstein equation are unreasonably small, while aggregate radii and aggregation numbers obtained from the ratio of self-diffusion coefficients are more in line with data on a similar system reported in the literature. 3,14,19,66-

DISCUSSION

The results from this study confirm the prior findings on the binary system C₁₀E₆ in cyclohexane (no water added) that the Stokes-Einstein equation fails to provide reasonable aggregate radii for this reverse micelle-forming system. ¹⁷ This finding was attributed to a change in mass-transport process from the movement of the small reverse micelles at low surfactant concentration to individual C₁₀E₆ molecules jumping from reverse micelle to reverse micelle at high surfactant concentration. Additional insights can be derived from the observation in this study that the cyclohexane self-diffusion coefficient is independent from the amount of present water. In other words, the added water does not interfere with the translational motion of the cyclohexane. This makes sense in so far that the water clearly resides within the reverse micelle, given the observed small self-diffusion coefficients, and is thus shielded from the cyclohexane. However, the data in this study confirm the findings made by others 14,71,72 that the average aggregation number of the reverse micelles increases exponentially with water load. Thus, the size of the reverse micelles apparently has also no influence on the translational motion of cyclohexane. This might be explained by a cancellation of two effects. While larger reverse micelles may block translational motion of the cyclohexane in the continuous phase more so than smaller reverse micelles do, larger reverse micelles should require more surfactant molecules and at constant overall surfactant concentration, there are fewer reverse micelles that hinder the translational motion of the cyclohexane. All the more remarkable it is that the solution viscosity is a strongly increasing function with water load. Reverse micelle size has thus a strong influence on solution viscosity. Hence, these observed trends show a strong decoupling of solution viscosity from the translational motion of the cyclohexane continuous phase. Such decoupling of viscosity and translational motion has been a key feature in many other systems, where a breakdown of the Stokes-Einstein equation has been observed. Specifically, in supercooled and glass-forming systems, the viscosity is often observed to decouple from self-diffusion below a certain critical temperature. While self-diffusion remains comparably fast, viscosity dramatically increases in these systems, which

then results in the breakdown of the Stokes–Einstein equation, ^{22,23} just as observed in this study here.

The critical temperature at which this decoupling starts to occur in supercooled and glass-forming systems may at times be surprisingly high and be above the glass-transition temperature or melting temperature as observed, for example, for water, 44 phase-change materials, 34 several ionic liquids, 40 and GeTe alloy, where in the latter case high atomic mobility above T_g was found in large-scale molecular dynamics (MD) simulations.33 In theoretical treatments of glass-forming liquids, it was argued that the Stokes-Einstein breakdown is caused by a spatial heterogeneity of dynamics. 73,74 We note that short-range ordering has also been implicated as a root for deviations from the Stokes-Einstein equation, 75 in particular five-fold icosahedral short-range order for metallic glass formers^{24,28,30} as well as water aggregates around dimethylsulfoxide and ethanol in respective liquid-liquid binary systems. 49 Nevertheless, efforts are ongoing to obtain a more detailed understanding of these glass systems that contain the presence of dynamic heterogeneity. 76 For example, coexisting regions of cage rattling-dominant motions and jump-dominated motions have been found in MD studies of supercooled GeTe.³² Hopping motions have been found in a theoretical study to induce a breakdown of the Stokes-Einstein equation for a simple structural glass-former model, the infinite-range variant of the hard sphere based model.⁷⁷ Translational jump diffusion has also been noted as a key feature in supercooled water 43,44 that could be described by the elastically collective nonlinear Langevin equation theory that incorporates such local hopping.⁴³ Removal of translational jump diffusion from the overall obtained self-diffusion coefficient in MD simulations in supercooled water led to a residual diffusion coefficient that continued to be coupled very strongly with viscosity. 44 A similar coexistence of two modes of diffusion motions (rattling within a cavity and hopping motions) can be expected to be present in the reverse micellar system studied here. The dynamics for the C₁₀E₆ being part of a reverse micelle must clearly be different from the dynamics of the cyclohexane continuous phase. It is conceivable that the motions of C₁₀E₆ may be described by a coexistence of a "rattling" motion within the reverse micelle and a "hopping" motion between reverse micelles. The hopping motion provides a basis for the hypothesis we formulate next and pictorially display in Figure 7 to explain the nonuniformity of the polydisperse C₁₀E₆ selfdiffusion at higher water loads, leading to the spread-out cross peak of the proton signal from the ethylene oxide repeat unit observed in the 2D-DOSY spectrum in Figure 2.

Prior $C_m E_n$ concentration studies have shown that the surfactant molecules assemble in a step-wise fashion resulting in an absence of a sharp critical micelle concentration and that substantial amounts of C_mE_n molecules are not incorporated into reverse micelles even at high $C_m E_n$ concentrations. ^{16,17} Thus, in the samples studied here, we hypothesize that the overall $C_m E_n$ translational motion is dominated by reverse micelle to reverse micelle "hopping" motions. At low water loads, all C_mE_n molecules can participate in these "hopping" motions. Thus, the NMR self-diffusion data reflect the time and ensemble average of the motions of all $C_m E_n$ molecules present in the polydisperse C₁₀E₆. As the water load increases, the additional water molecules provide strong hydrogen bonding interactions with the hydroxyl group as well as with the ether oxygens of the ethylene oxide repeat unit of $C_{10}E_6$. In fact, the strength of these hydrogen bonding interactions has

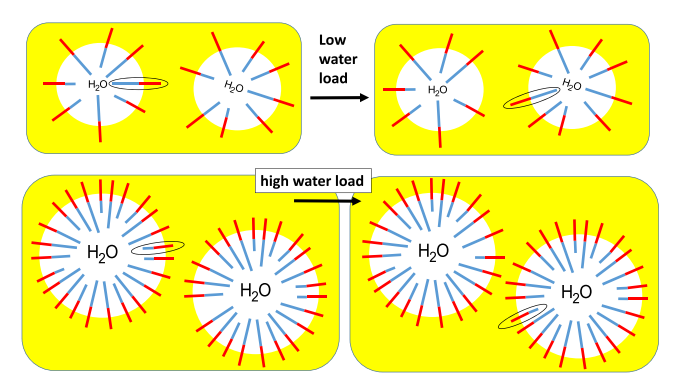


Figure 7. Sketch to illustrate the hypothesis that dynamics in the polydisperse $C_{10}E_6$ in cyclohexane (yellow representing the continuous solvent phase) reverse micelle system is dominated by reverse micelle to reverse micelle "hopping" motions. At low water load (indicated by small font size), all C_mE_n molecules can participate. At high water load (indicated by large font size), only C_mE_n molecules with short ethylene oxide repeat units can participate. The different lengths of the blue colored sticks in the sketch illustrate the polydispersity of the ethylene oxide repeat unit.

been demonstrated in several experimental and theoretical studies. In an NMR titration study of "dry" polydisperse C₉E₅ with water, two water resonances were observed at very low water load representing water hydrogen bonded between the $C_m E_n$ ether oxygens and water in fast chemical exchange with the $C_m E_n$ hydroxyl proton. 18 MD simulations noticed also intramolecular bridging hydrogen bonds in aqueous solutions of $C_m E_n^{78,79}$ In a study of gas solubility in reverse micellar systems of the related surfactant Triton X-100 in cyclohexane, 80 the authors deduced that the formation of a water pool commences only at water loads of 3, which implies that water resides preferentially between the ethylene oxide chains at lower water loads. Finally, a study of the interfacial hydrogen bonding dynamics in reverse micelles of nonpolar sorbitan monostearate (Span-60) in *n*-octane revealed that a greater amount of water penetrates the surfactant region and that further addition of water leads to a deeper penetration with associated observed slowdown of hydrogen bonding fluctuations.⁸¹ Therefore, strong hydrogen bonding interactions are likely present within the reverse micelle core, which would lead to a tying of neighboring $C_m E_n$ molecules by bridging hydrogen bonds directly between ether/hydroxy oxygens as well as indirectly through chains of hydrogen bonded water molecules. Thus, the added water within the reverse micelle core acts like a glue between the $C_{10}E_6$ molecules within the reverse micellar core. The core also increases in size with increasing amounts of water in the system requiring, according to Figure 6, an exponentially increasing number of surfactant molecules to envelop the core within the micelle. The $C_m E_n$ with shorter ethylene oxide chains will not reach as far into the water pool as the ones with longer ethylene oxide chains, as their hydrophobic alkyl chain will stay within the hydrophobic surface layer formed as part of the reverse micelle. Thus, at high water load, only $\hat{C}_m E_n$ molecules with short ethylene oxide chains are primarily participating in the reverse micelle to reverse micelle hopping motion, while the $C_m E_n$ molecules with long ethylene oxide chains primarily remain within the micelle. It is important here to realize that all $C_m E_n$ molecules possess the same alkyl chain, but only $C_m E_n$ molecules with long ethylene oxide chains contain these associated protons. Thus, while the cross peaks in the 2D-DOSY graph of Figure 2

associated with the alkyl chain reflect the time and ensemble average of all C_mE_n molecules, the spread-out 2D-DOSY ethylene oxide signal reflects the $C_m E_n$ molecules with long ethylene oxide chains that primarily remain within the micelles and thus diffuse significantly slower. This implies that the residence times of these large $C_m E_n$ molecules in the reverse micelle have to be at least on the order of milliseconds to be separately visible on a time scale of the NMR experiment.⁸² For the sample with monodisperse C₁₀E₆, there is only one distinct $C_m E_n$ molecule and naturally the differentiation between C_mE_n molecules with shorter and longer ethylene oxide repeat units is absent. Consequently, no spread of cross peaks but only one cross peak is observed for the protons from the ethylene oxide repeat unit in Figure S7 in the Supporting Information. We note that the self-diffusion coefficients for the water (Table S7), which is trapped within the reverse micellar core, appear to be even slower than the average polydisperse $C_{10}E_6$ self-diffusion coefficients (Table S4). This is even more clearly observed for the sample prepared with the monodisperse $C_{10}E_6$.

Thus, in light of the presence of these dynamic heterogeneities in this studied reverse micellar system, it is not surprising after all that unreasonable reverse micelle radii and aggregation numbers result from employing the Stokes—Einstein equation. When taking the ratio of surfactant and cyclohexane self-diffusion coefficients to evaluate the reverse micellar radii, the effect of the solution viscosity is removed as this value does not even enter into the calculation. Thus, different values for radii and aggregation numbers result from taking the ratio of self-diffusion coefficients of surfactant and cyclohexane. These radii appear to be more in line with values reported for similar systems using other experimental techniques. Future studies beyond the scope of this report, such as DLS studies or MD simulations, would be helpful to gain additional structural and dynamic information.

In light of the breakdown of the Stokes-Einstein equation observed in the reverse micellar system studied here, it is interesting that Arrhenius temperature dependence is evident for the self-diffusion coefficients for all species as well as the solution viscosity. This is contrary to the behavior observed in metallic glass-forming liquids. Specifically, Hu et al.⁸³ observed for three metallic glass-forming liquids in MD simulation studies an evolution of microstructure and concurrent crossover from Arrhenius to non-Arrhenius behavior at temperatures higher than the temperatures where the Stokes-Einstein equation breaks down. Lee and Vlassak²⁶ observed by nanocalorimetry that diffusion kinetics in CuZr and NiZr alloys changed from non-Arrhenius in the supercooled liquid state to Arrhenius in the solid state. However, Arrhenius behavior was obtained in an MD study for the selfdiffusion of nitrate in aqueous solution, for which translationalrotational coupling was proposed as the reason for the breakdown of the Stokes-Einstein equation.⁵¹

Perhaps most revealing here is a study on supercooled aqueous glycerol solutions, which observed the presence of a liquid—liquid transition for a water-rich mixture and pointed out that its influence on the dynamics was not known yet. A similar situation is present in the reverse micellar solutions in cyclohexane studied here. We observed a liquid—liquid phase transition at 6–7 mass percent added water ($W \approx 11$) at ambient conditions. This points toward one distinguishing feature of the reverse micelle system studied here to the abovementioned systems cited from the literature, which is the

nature of the associated phase transition. The reverse micelle system studied here is close to a liquid—liquid phase transition, while the glass-forming systems discussed above are close to liquid-to-solid (glass) transition. Possibly, the temperature dependence remains to be of Arrhenius-type in systems near liquid—liquid phase transitions because all involved phases are liquid phases where no motions are frozen out. We are not aware of relevant studies on other systems near a liquid—liquid phase transition that inspect the validity of the Stokes—Einstein equation and deviations of the Arrhenius-type temperature dependence. Thus, this aspect appears to be an interesting subject for future studies.

CONCLUSIONS

The validity of the Stokes-Einstein equation was evaluated and found to produce unreasonably small reverse micelle radii and average aggregation numbers for the system of C₁₀E₆ in cyclohexane with varying amounts of added water. However, reasonable values for these quantities were obtained using the ratio of surfactant to cyclohexane self-diffusion coefficients. The cyclohexane self-diffusion coefficients were found to be independent of the amount of added water, while the selfdiffusion coefficients of surfactant and water decreased with increasing water load. Viscosity also increased with increasing water load, illustrating a strong decoupling of the solution viscosity and the cyclohexane self-diffusion. Such decoupling of viscosity and self-diffusion is typical for systems that exhibit a breakdown of the Stokes-Einstein equation. It was presumed that reverse micelle to reverse micelle hopping motions dominate translational mass transport at the studied surfactant solutions. The observed spread of self-diffusion coefficients of the ethylene oxide repeat unit in polydisperse $C_m E_n$ in the reverse micellar system at higher water load was explained with a preferential resistance to the reverse micelle to reverse micelle hopping motion by the $C_m E_n$ molecules with a large number of ethylene oxide repeat units because of stronger hydrogen bonding interactions with the core water molecules. In spite of the evidence of decoupling of viscosity and selfdiffusion and the presence of heterogeneous dynamics, the temperature dependence was found to follow Arrhenius behavior over the investigated range of temperatures. It would be interesting to investigate other systems with aggregation propensities near liquid to liquid phase transitions to test if a breakdown of the Stokes-Einstein equation would be observed without deviations from the Arrhenius law.

ASSOCIATED CONTENT

Supporting Information

The Supporting Information is available free of charge at https://pubs.acs.org/doi/10.1021/acs.jpcb.0c06124.

Sample preparation details, tabulated values of density, viscosity, self-diffusion, reverse micelle radii and aggregation numbers as well as associated uncertainties, proton NMR spectrum with spectral assignment, exemplary graphs of analyzing $C_{10}E_6$ self-diffusion data, and 2D-DOSY spectrum of a sample prepared with monodisperse $C_{10}E_6$ (PDF)

AUTHOR INFORMATION

Corresponding Authors

Markus M. Hoffmann – Department of Chemistry and Biochemistry, State University of New York College at Brockport, Brockport, New York 14420, United States;
orcid.org/0000-0002-5469-8665; Phone: +(585) 395-5587; Email: mhoffman@brockport.edu; Fax: +(585) 395-5805

Gerd Buntkowsky — Institute of Physical Chemistry, Technical University Darmstadt, Darmstadt D-64287, Germany;
orcid.org/0000-0003-1304-9762; Phone: +49 6151 16-21116; Email: gerd.buntkowsky@chemie.tu-darmstadt.de;
Fax: +49 6151 16-21119

Authors

Matthew D. Too — Department of Chemistry and Biochemistry, State University of New York College at Brockport, Brockport, New York 14420, United States

Michael Vogel — Institute of Condensed Matter Physics, Technical University Darmstadt, Darmstadt 64289, Germany; orcid.org/0000-0003-2706-3522

Torsten Gutmann − *Institute of Physical Chemistry, Technical University Darmstadt, Darmstadt D-64287, Germany;* orcid.org/0000-0001-6214-2272

Complete contact information is available at: https://pubs.acs.org/10.1021/acs.jpcb.0c06124

Notes

The authors declare no competing financial interest.

ACKNOWLEDGMENTS

This report is based upon work supported by the National Science Foundation under grant no. [1953428] and the Deutsche Forschungsgemeinschaft (DFG) under grant Bu 911/24-2. The latter included a Mercator fellowship for M.M.H. to support research stays at the Technical University Darmstadt. M.D.T. is grateful for receiving the Morris Fellowship for Summer Research in Chemistry. We thank Rochester Midland Corporation for donating the industrial $C_{10}E_{6}$ polydisperse surfactant.

■ REFERENCES

- (1) Somasundaran, P. Encyclopedia of Surface and Colloid Science, 3rd ed.; CRC Press: Boca Raton, 2015.
- (2) Khoshnood, A.; Firoozabadi, A. Polar solvents trigger formation of reverse micelles. *Langmuir* **2015**, *31*, 5982–5991.
- (3) Lemyre, J.-L.; Lamarre, S.; Beaupré, A.; Ritcey, A. M. A new approach for the characterization of reverse micellar systems by dynamic light scattering. *Langmuir* **2010**, *26*, 10524–10531.
- (4) Vasquez, V. R.; Williams, B. C.; Graeve, O. A. Stability and comparative analysis of aot/water/isooctane reverse micelle system using dynamic light scattering and molecular dynamics. *J. Phys. Chem. B* **2011**, *115*, 2979–2987.
- (5) Abel, S.; Galamba, N.; Karakas, E.; Marchi, M.; Thompson, W. H.; Laage, D. On the structural and dynamical properties of DOPC reverse micelles. *Langmuir* **2016**, 32, 10610–10620.
- (6) Das, A.; Patra, A.; Mitra, R. K. Do the physical properties of water in mixed reverse micelles follow a synergistic effect: A spectroscopic investigation. *J. Phys. Chem. B* **2013**, 117, 3593–3602.
- (7) Pal, N.; Verma, S. D.; Singh, M. K.; Sen, S. Fluorescence correlation spectroscopy: An efficient tool for measuring size, size-distribution and polydispersity of microemulsion droplets in solution. *Anal. Chem.* **2011**, *83*, 7736–7744.
- (8) Burnett, G. R.; Rees, G. D.; Steytler, D. C.; Robinson, B. H. Fluorescence correlation spectroscopy of water-in-oil microemulsions: An application in specific characterisation of droplets containing biomolecules. *Colloids Surf., A* **2004**, *250*, 171–178.

- (9) Pérez, S.; Olea, A.; Gárate, M. Formation and morphology of reverse micelles formed by nonionic surfactants in "dry" organic solvents. *Curr. Topics Medic. Chem.* **2014**, *14*, 774–780.
- (10) Sandoval, T. E.; Espinoza, L. J.; Guerra, I. A.; Olea, A. F.; Gárate, M. P. Study of the size and morphology of aggregates formed by pentaethylene glycol monooctyl ether (C_8EO_5) in n-heptane. *Colloids Surf., A* **2012**, 398, 17–23.
- (11) Mills, A. J.; Wilkie, J.; Britton, M. M. NMR and molecular dynamics study of the size, shape, and composition of reverse micelles in a cetyltrimethylammonium bromide (CTAB)/n-hexane/pentanol/water microemulsion. *J. Phys. Chem. B* **2014**, *118*, 10767–10775.
- (12) Sugioka, H.; Matsuoka, K.; Moroi, Y. Temperature effect on formation of sodium cholate micelles. *J. Colloid Interface Sci.* **2003**, 259, 156–162.
- (13) Attwood, D. The mode of association of amphiphilic drugs in aqueous solution. *Adv. Colloid Interface Sci.* **1995**, *55*, 271–303.
- (14) Vasilescu, M.; Caragheorgheopol, A.; Almgren, M.; Brown, W.; Alsins, J.; Johannsson, R. Structure and dynamics of nonionic polyoxyethylenic reverse micelles by time-resolved fluorescence quenching. *Langmuir* 1995, 11, 2893–2898.
- (15) Fendler, J. H. Interactions and reactions in reversed micellar systems. *Acc. Chem. Res.* **1976**, *9*, 153–161.
- (16) Smith, G. N.; Brown, P.; Rogers, S. E.; Eastoe, J. Evidence for a critical micelle concentration of surfactants in hydrocarbon solvents. *Langmuir* **2013**, 29, 3252–3258.
- (17) Hoffmann, M. M.; Bothe, S.; Gutmann, T.; Buntkowsky, G. Combining freezing point depression and self-diffusion data for characterizing aggregation. *J. Phys. Chem. B* **2018**, *122*, 4913–4921.
- (18) Hoffmann, M. M.; Bennett, M. E.; Fox, J. D.; Wyman, D. P. Water partitioning in "dry" poly(ethylene oxide) alcohol ($C_m E_n$) nonionic surfactant-a proton NMR study. *J. Colloid Interface Sci.* **2005**, 287, 712–716.
- (19) Shrestha, L. K.; Shrestha, R. G.; Oyama, K.; Matsuzawa, M.; Aramaki, K. Structure of diglycerol polyisostearate nonionic surfactant micelles in nonpolar oil hexadecane: A SAXS study. *J. Oleo Sci.* **2010**, 59, 339–350.
- (20) Ganguli, A. K.; Ganguly, A.; Vaidya, S. Microemulsion-based synthesis of nanocrystalline materials. *Chem. Soc. Rev.* **2010**, *39*, 474–485.
- (21) Sharma, S.; Pal, N.; Chowdhury, P. K.; Sen, S.; Ganguli, A. K. Understanding growth kinetics of nanorods in microemulsion: A combined fluorescence correlation spectroscopy, dynamic light scattering, and electron microscopy study. *J. Am. Chem. Soc.* **2012**, 134, 19677–19684.
- (22) Chang, I.; Fujara, F.; Geil, B.; Heuberger, G.; Mangel, T.; Sillescu, H. Translational and rotational molecular motion in supercooled liquids studied by NMR and forced rayleigh scattering. *J. Non-Cryst. Solids* **1994**, *172–174*, 248–255.
- (23) Cicerone, M. T.; Ediger, M. D. Enhanced translation of probe molecules in supercooled o-terphenyl: Signature of spatially heterogeneous dynamics? *J. Chem. Phys.* **1996**, *104*, 7210–7218.
- (24) Pasturel, A.; Jakse, N. Short-range structural signature of transport properties of Al-Ni melts. *J. Non-Cryst. Solids* **2015**, 425, 176–182.
- (25) Schmelzer, J. W. P.; Abyzov, A. S.; Fokin, V. M.; Schick, C.; Zanotto, E. D. Crystallization in glass-forming liquids: Effects of decoupling of diffusion and viscosity on crystal growth. *J. Non-Cryst. Solids* **2015**, 429, 45–53.
- (26) Lee, D.; Vlassak, J. J. Diffusion kinetics in binary CuZr and NiZr alloys in the super-cooled liquid and glass states studied by nanocalorimetry. *Scr. Mater.* **2019**, *165*, 73–77.
- (27) Lee, D.; et al. Crystallization behavior upon heating and cooling in Cu50Zr50 metallic glass thin films. *Acta Mater.* **2016**, *121*, 68–77.
- (28) Li, C. H.; Luan, Y. W.; Han, X. J.; Li, J. G. Structural aspects of the Stokes-Einstein relation breakdown in high temperature melts. *J. Non-Cryst. Solids* **2017**, *458*, 107–117.
- (29) An, S.; Li, Y.; Li, J.; Zhao, S.; Liu, B.; Guan, P. The linear relationship between diffusivity and crystallization kinetics in a deeply supercooled liquid Ni50Ti50 alloy. *Acta Mater.* **2018**, *152*, 1–6.

- (30) Puosi, F.; Pasturel, A. Nucleation kinetics in a supercooled metallic glass former. *Acta Mater.* **2019**, *174*, 387–397.
- (31) Zhou, Y. H.; Han, X. J.; Li, J. G. Transport properties and abnormal breakdown of the Stokes-Einstein relation in computer simulated Al₇₂Ni₁₆Co₁₂ metallic melt. *J. Non-Cryst. Solids* **2019**, *517*, 83–95.
- (32) Sosso, G. C.; Colombo, J.; Behler, J.; Del Gado, E.; Bernasconi, M. Dynamical heterogeneity in the supercooled liquid state of the phase change material GeTe. *J. Phys. Chem. B* **2014**, *118*, 13621–13628
- (33) Sosso, G. C.; Miceli, G.; Caravati, S.; Giberti, F.; Behler, J.; Bernasconi, M. Fast crystallization of the phase change compound GeTe by large-scale molecular dynamics simulations. *J. Phys. Chem. Lett.* **2013**, *4*, 4241–4246.
- (34) Wei, S.; Evenson, Z.; Stolpe, M.; Lucas, P.; Angell, C. A. Breakdown of the Stokes-Einstein relation above the melting temperature in a liquid phase-change material. *Sci. Adv.* **2018**, *4*, No. eaat8632.
- (35) Wojnarowska, Z.; et al. Experimental evidence of high pressure decoupling between charge transport and structural dynamics in a protic ionic glass-former. *Sci. Rep.* **2017**, *7*, 7084.
- (36) Lee, E.; Jung, Y. Slow dynamics of ring polymer melts by asymmetric interaction of threading configuration: Monte Carlo study of a dynamically constrained lattice model. *Polymers* **2019**, *11*, 516.
- (37) Maldonado-Camargo, L.; Rinaldi, C. Breakdown of the Stokes-Einstein relation for the rotational diffusivity of polymer grafted nanoparticles in polymer melts. *Nano Lett.* **2016**, *16*, *6767–6773*.
- (38) Hung, J.-H.; Mangalara, J. H.; Simmons, D. S. Heterogeneous rouse model predicts polymer chain translational normal mode decoupling. *Macromolecules* **2018**, *51*, 2887–2898.
- (39) Alam, T. M.; Dreyer, D. R.; Bielawski, C. W.; Ruoff, R. S. Combined measurement of translational and rotational diffusion in quaternary acyclic ammonium and cyclic pyrrolidinium ionic liquids. *J. Phys. Chem. B* **2013**, *117*, 1967–1977.
- (40) Hensel-Bielowka, S.; et al. Heterogeneous nature of relaxation dynamics of room-temperature ionic liquids (EMIm)₂[Co(NCS)₄] and (BMIm)₂[Co(NCS)₄]. *J. Phys. Chem. C* **2015**, *119*, 20363–20368.
- (41) Becher, M.; Steinrücken, E.; Vogel, M. On the relation between reorientation and diffusion in glass-forming ionic liquids with microheterogeneous structures. *J. Chem. Phys.* **2019**, *151*, 194503.
- (42) Walker, J. A.; Mezyk, S. P.; Roduner, E.; Bartels, D. M. Isotope dependence and quantum effects on atomic hydrogen diffusion in liquid water. *J. Phys. Chem. B* **2016**, *120*, 1771–1779.
- (43) Klameth, F.; Vogel, M. Slow water dynamics near a glass transition or a solid interface: A common rationale. *J. Phys. Chem. Lett.* **2015**, *6*, 4385–4389.
- (44) Dueby, S.; Dubey, V.; Daschakraborty, S. Decoupling of translational diffusion from the viscosity of supercooled water: Role of translational jump diffusion. *J. Phys. Chem. B* **2019**, 123, 7178–7189.
- (45) Świergiel, J.; Plowas, I.; Grembowski, J.; Jadzyn, J. Stokes-Einstein-Nernst relation in dilute electrolyte solutions of lithium perchlorate in polyethylene glycols (200, 300, 400, and 600). *J. Chem. Eng. Data* **2015**, *60*, 3588–3593.
- (46) Prasad, S.; Chakravarty, C.; Kashyap, H. K. Concentration-dependent structure and dynamics of aqueous LiCl solutions: A molecular dynamics study. *J. Mol. Liq.* **2017**, 225, 240–250.
- (47) Schneider, S.; Vogel, M. NMR studies on the coupling of ion and water dynamics on various time and length scales in glass-forming LiCl aqueous solutions. *J. Chem. Phys.* **2018**, *149*, 104501.
- (48) González, J. A. T.; Longinotti, M. P.; Corti, H. R. Diffusion-viscosity decoupling in supercooled glycerol aqueous solutions. *J. Phys. Chem. B* **2015**, *119*, 257–262.
- (49) Kumar, S.; Sarkar, S.; Bagchi, B. Microscopic origin of breakdown of Stokes-Einstein relation in binary mixtures: Inherent structure analysis. *J. Chem. Phys.* **2020**, *152*, 164507.
- (50) Kumar, S.; Sarkar, S.; Bagchi, B. Anomalous viscoelastic response of water-dimethyl sulfoxide solution and a molecular

- explanation of non-monotonic composition dependence of viscosity. *J. Chem. Phys.* **2019**, *151*, 194505.
- (51) Banerjee, P.; Yashonath, S.; Bagchi, B. Rotation driven translational diffusion of polyatomic ions in water: A novel mechanism for breakdown of Stokes-Einstein relation. *J. Chem. Phys.* **2017**, *146*, 164502.
- (52) Bastelberger, S.; Krieger, U. K.; Luo, B.; Peter, T. Diffusivity measurements of volatile organics in levitated viscous aerosol particles. *Atmos. Chem. Phys.* **2017**, *17*, 8453–8471.
- (53) Yang, X.; Feng, Y.; Xu, J.; Jin, J.; Liu, Y.; Cao, B. Numerical study on transport properties of the working mixtures for coal supercritical water gasification based power generation systems. *Appl. Therm. Eng.* **2019**, *162*, 114228.
- (54) Turton, D. A.; Wynne, K. Stokes-Einstein-Debye failure in molecular orientational diffusion: Exception or rule? *J. Phys. Chem. B* **2014**, *118*, 4600–4604.
- (55) Hoffmann, M. M.; Bothe, S.; Gutmann, T.; Hartmann, F.-F.; Reggelin, M.; Buntkowsky, G. Directly vs indirectly enhanced ¹³C in dynamic nuclear polarization magic angle spinning NMR experiments of nonionic surfactant systems. *J. Phys. Chem. C* **2017**, *121*, 2418–2427
- (56) Van Geet, A. L. Calibration of the methanol and glycol nuclear magnetic resonance thermometers with a static thermister probe. *Anal. Chem.* **1968**, *40*, 2227–2229.
- (57) Jerschow, A.; Müller, N. 3D diffusion-ordered TOCSY for slowly diffusing molecules. J. Magn. Reson. A 1996, 123, 222–225.
- (58) Jerschow, A.; Müller, N. Suppression of convection artifacts in stimulated-echo diffusion experiments. Double-stimulated-echo experiments. J. Magn. Reson. 1997, 125, 372–375.
- (59) Nicolay, K.; Braun, K. P. J.; Graaf, R. A. d.; Dijkhuizen, R. M.; Kruiskamp, M. J. Diffusion NMR spectroscopy. NMR Biomed. 2001, 14, 94–111.
- (60) Chen, H. C.; Chen, S. H. Diffusion of crown ethers in alcohols. *J. Phys. Chem.* **1984**, *88*, 5118–5121.
- (61) Gierer, A.; Wirtz, K. Molecular theory of microfriction. Z. Naturforsch. A 1953, 8, 532–538.
- (62) Clark, S.; Fletcher, P. D. I.; Ye, X. Interdroplet exchange rates of water-in-oil and oil-in-water microemulsion droplets stabilized by pentaoxyethylene monododecyl ether. *Langmuir* **1990**, *6*, 1301–1309.
- (63) Fletcher, P. D. I.; Horsup, D. I. Droplet dynamics in water-inoil microemulsions and macroemulsions stabilized by non-ionic surfactants. *J. Chem. Soc. Faraday Trans.* **1992**, *88*, 855–864.
- (64) Bondi, A. Van der waals volumes and radii. J. Phys. Chem. 1964, 68, 441–451.
- (65) Edward, J. T. Molecular volumes and the Stokes-Einstein equation. J. Chem. Educ. 1970, 47, 261–270.
- (66) Dutta, C.; Svirida, A.; Mammetkuliyev, M.; Rukhadze, M.; Benderskii, A. V. Insight into water structure at the surfactant surfaces and in microemulsion confinement. *J. Phys. Chem. B* **2017**, *121*, 7447–7454.
- (67) Shrestha, L. K.; Shrestha, R. G.; Aramaki, K.; Yoshikawa, G.; Ariga, K. Demonstration of solvent-induced one-dimensional non-ionic reverse micelle growth. *J. Phys. Chem. Lett.* **2013**, *4*, 2585–2590.
- (68) Shrestha, L. K.; Glatter, O.; Aramaki, K. Structure of nonionic surfactant (glycerol α -monomyristate) micelles in organic solvents: A SAXS study. *J. Phys. Chem. B* **2009**, *113*, 6290–6298.
- (69) Shrestha, L. K.; Aramaki, K. Structural investigation of diglycerol monolaurate reverse micelles in nonpolar oils cyclohexane and octane. *J. Oleo Sci.* **2009**, *58*, 235–242.
- (70) Shrestha, L. K.; Sato, T.; Aramaki, K. Intrinsic parameters for structural variation of reverse micelles in nonionic surfactant (glycerol α -monolaurate)/oil systems: A SAXS study. *Phys. Chem. Chem. Phys.* **2009**, *11*, 4251–4259.
- (71) Sjöblom, J. Model calculations of aggregation numbers and radii of w/o microemulsions. *Colloid & Polymer Sci.* **1980**, 258, 1164–1170
- (72) Arleth, L.; Svensson, B.; Mortensen, K.; Pedersen, J. S.; Olsson, U. Block-copolymer micro-emulsion with solvent-induced segregation. *Langmuir* **2007**, 23, 2117–2125.

- (73) Ediger, M. D. Spatially heterogeneous dynamics in supercooled liquids. *Annu. Rev. Phys. Chem.* **2000**, *51*, 99–128.
- (74) Sillescu, H. Heterogeneity at the glass transition: A review. J. Non-Cryst. Solids 1999, 243, 81–108.
- (75) Pan, S.; Wu, Z. W.; Wang, W. H.; Li, M. Z.; Xu, L. Structural origin of fractional Stokes-Einstein relation in glass-forming liquids. *Sci. Rep.* **2017**, *7*, 39938.
- (76) Pastore, R.; Coniglio, A.; Ciamarra, M. P. Dynamic phase coexistence in glass-forming liquids. *Sci. Rep.* **2015**, *5*, 11770.
- (77) Charbonneau, P.; Jin, Y.; Parisi, G.; Zamponi, F. Hopping and the Stokes-Einstein relation breakdown in simple glass formers. *Proc. Natl. Acad. Sci. U.S.A.* **2014**, *111*, 15025–15030.
- (78) Tasaki, K. Poly(oxyethylene)—water interactions: A molecular dynamics study. *J. Am. Chem. Soc.* **1996**, *118*, 8459–8469.
- (79) Horta, B. A. C.; Merz, P. T.; Fuchs, P. F. J.; Dolenc, J.; Riniker, S.; Hünenberger, P. H. A gromos-compatible force field for small organic molecules in the condensed phase: The 2016h66 parameter set. J. Chem. Theory Comput. 2016, 12, 3825–3850.
- (80) Shen, D.; Zhang, R.; Han, B.; Dong, Y.; Wu, W.; Zhang, J.; Li, J.; Jiang, T.; Liu, Z. Enhancement of the solubilization capacity of water in Triton X-100/cyclohexane/water system by compressed gases. *Chem.—Eur. J.* **2004**, *10*, 5123–5128.
- (81) Baryiames, C. P.; Teel, M.; Baiz, C. R. Interfacial h-bond dynamics in reverse micelles: The role of surfactant heterogeneity. *Langmuir* **2019**, *35*, 11463–11470.
- (82) Sanders, J. K. M.; Hunter, B. K. Modern NMR Spectroscopy-a Guide for Chemists; Oxford University Press: New York, 1993.
- (83) Hu, Y. C.; Li, F. X.; Li, M. Z.; Bai, H. Y.; Wang, W. H. Structural signatures evidenced in dynamic crossover phenomena in metallic glass-forming liquids. *J. Appl. Phys.* **2016**, *119*, 205108.